Title
Nonmonotonic Energy Dependence of Net-Proton Number Fluctuations

Permalink
https://escholarship.org/uc/item/19m4w50f

Journal
Physical Review Letters, 126(9)

ISSN
0031-9007

Authors
Adam, J
Adamczyk, L
Adams, JR
et al.

Publication Date
2021-03-05

DOI
10.1103/physrevlett.126.092301

Peer reviewed

Non-monotonic energy dependence of net-proton number fluctuations

J. Adam[6], L. Adamczyk[2], J. R. Adams[39], J. K. Adkins[30], G. Agakishiev[28], M. M. Aggarwal[41], Z. Ahammed[61], I. Alekseev[3,35], D. M. Anderson[55], A. Aparin[28], E. C. Aschenauer[6], M. U. Ashraf[11], F. G. Atetalla[29], A. Attri[41], G. S. Averichev[28], V. Bairathi[53], K. Barish[10], A. Behera[52], R. Bellwied[20], A. Bhasin[27], J. Bielcik[14], J. Bielcikova[38], L. C. Bland[6], I. G. Bordyuzhin[3], J. D. Brandenburg[6], A. V. Brandin[35], J. Butterworth[45], H. Caines[64], M. Calderón de la Barca Sánchez[8], D. Cebra[8], I. Chakaberia[29,6], P. Chaloupka[14], B. K. Chan[9], F-H. Chang[37], Z. Chang[6], N. Chankova-Bunzarova[28], A. Chatterjee[11], D. Chen[10], J. Chen[49], J. H. Chen[18], X. Chen[48], Z. Chen[49], J. Cheng[57], M. Cherney[13], M. Chevalier[10], S. Choudhury[18], W. Christie[6], X. Chu[6], H. J. Crawford[7], M. Csanád[16], T. G. Dedovich[28], I. M. Deppner[19], A. A. Derevschikov[43], L. Didenko[6], X. Dong[31], J. L. Drachenberg[1], J. C. Dunlop[6], T. Edmonds[44], N. Elsey[63], J. Engelage[7], G. Eppley[45], S. Esumi[58], O. Evdokimov[12], A. Ewigleben[32], O. Eyser[6], R. Fatemi[30], S. Fazio[6], P. Federic[38], J. Fedorisin[28], C. J. Feng[37], Y. Feng[44], P. Filip[28], E. Finch[51], Y. Fisyak[6], A. Francisco[64], L. Fulek[2], C. A. Gagliardi[55], T. Galatyuk[15], F. Geurts[45], A. Gibson[60], K. Gopal[23], X. Gou[49], D. Grosnick[60], W. Guryn[6], A. I. Hamad[29], A. Hamed[5], S. Harabasz[15], J. W. Harris[64], S. He[11], W. He[18], X. H. He[26], Y. He[49], S. Heppelmann[8], S. Heppelmann[42], N. Herrmann[19], E. Hoffman[20], L. Holub[14], Y. Hong[31], S. Horvat[64], Y. Hu[18], H. Z. Huang[9], S. L. Huang[52], T. Huang[37], X. Huang[57], T. J. Humanic[39], P. Huo[52], G. Igo[9], D. Isenhower[1], W. W. Jacobs[25], C. Jena[23], A. Jentsch[6], Y. JI[48], J. Jia[6,52], K. Jiang[48], S. Jowzaee[63], X. Ju[48], E. G. Judd[7], S. Kabana[53], M. L. Kabir[10], S. Kagamaster[32], D. Kalinkin[25], K. Kang[57], D. Kapukchyan[10], K. Kauder[6], H. W. Ke[6], D. Keane[29], A. Kechechyan[28], M. Kelsey[31], Y. V. Khyzhniak[35], D. P. Kikoła[62], C. Kim[10], B. Kimelman[8], D. Kincses[16], T. A. Kinghorn[8], I. Kisel[17], A. Kiselev[6], M. Kocan[14], L. Kochenda[35], L. K. Kosarzewski[14], L. Kramarik[14], P. Kravtsov[35], K. Krueger[4], N. Kulathunga Mudiyanselage[20], L. Kumar[41], S. Kumar[26], R. Kunnawalkam Elayavalli[63], J. H. Kwasizur[25], R. Lacey[52], S. Lan[11], J. M. Landgraf[6], J. Lauret[6], A. Lebedev[6], R. Lednicky[28], J. H. Lee[6], Y. H. Leung[31], C. Li[49], C. Li[48], W. Li[45], W. Li[50], X. Li[48], Y. Li[57], Y. Liang[29], R. Licenik[38], T. Lin[55], Y. Lin[11], M. A. Lisa[39], F. Liu[11], H. Liu[25], P. Liu[52], P. Liu[50], T. Liu[64], X. Liu[39], Y. Liu[55], Z. Liu[48], T. Ljubicic[6], W. J. Llope[63], R. S. Longacre[6], N. S. Lukow[54], S. Luo[12], X. Luo[11], G. L. Ma[50], L. Ma[18], R. Ma[6], Y. G. Ma[50], N. Magdy[12], R. Majka[64], D. Mallick[36], S. Margetis[29], C. Markert[56], H. S. Matis[31], J. A. Mazer[46], N. G. Minaev[43], S. Mioduszewski[55], B. Mohanty[36], I. Mooney[63], Z. Moravcova[14], D. A. Morozov[43], M. Nagy[16], J. D. Nam[54], Md. Nasim[22], K. Nayak[11], D. Neff[9], J. M. Nelson[7], D. B. Nemes[64], M. Nie[49], G. Nigmatkulov[35], T. Niida[58], L. V. Nogach[43], T. Nonaka[58], A. S. Nunes[6], G. Odyniec[31], A. Ogawa[6], S. Oh[31], V. A. Okorokov[35], B. S. Page[6], R. Pak[6], A. Pandav[36], Y. Panebratsev[28], B. Pawlik[40], D. Pawlowska[62], H. Pei[11], C. Perkins[7], L. Pinsky[20], R. L. Pintér[16], J. Pluta[62], J. Porter[31], M. Posik[54], N. K. Pruthi[41], M. Przybycien[2], J. Putschke[63], H. Qiu[26], A. Quintero[54], S. K. Radhakrishnan[29], S. Ramachandran[30], R. L. Ray[56], R. Reed[32], H. G. Ritter[31], O. V. Rogachevskiy[28], J. L. Romero[8], L. Ruan[6], J. Rusnak[38], N. R. Sahoo[49], H. Sako[58], S. Salur[46], J. Sandweiss[64], S. Sato[58], W. B. Schmidke[6], N. Schmitz[33], B. R. Schweid[52], F. Seck[15], J. Seger[13], M. Sergeeva[9], R. Seto[10], P. Seyboth[33], N. Shah[24], E. Shahaliev[28], P. V. Shanmuganathan[6], M. Shao[48], A. I. Sheikh[29], W. Q. Shen[50], S. S. Shi[11], Y. Shi[49], Q. Y. Shou[50], E. P. Sichtermann[31], R. Sikora[2], M. Simko[38], J. Singh[41], S. Singha[26], N. Smirnov[64], W. Solyst[25], P. Sorensen[6], H. M. Spinka[4], B. Srivastava[44], T. D. S. Stanislaus[60], M. Stefaniak[62], D. J. Stewart[64], M. Strikhanov[35], B. Stringfellow[44], A. A. P. Suaide[47], M. Sumbera[38], B. Summa[42], X. M. Sun[11], X. Sun[12], Y. Sun[48], Y. Sun[21], B. Surrow[54], D. N. Svirida[3], P. Szymanski[62], A. H. Tang[6], Z. Tang[48], A. Taranenko[35], T. Tarnowsky[34], J. H. Thomas[31], A. R. Timmins[20], D. Tlusty[13], M. Tokarev[28], C. A. Tomkiel[32], S. Trentalange[9], R. E. Tribble[55], P. Tribedy[6], S. K. Tripathy[16], O. D. Tsai[9], Z. Tu[6], T. Ullrich[6], D. G. Underwood[4], I. Upsal[49,6], G. Van Buren[6], J. Vanek[38], A. N. Vasiliev[43], I. Vassiliev[17], F. Videbæk[6], S. Vokal[28], S. A. Voloshin[63], F. Wang[44], G. Wang[9], J. S. Wang[21], P. Wang[48], Y. Wang[11], Y. Wang[57], Z. Wang[49], J. C. Webb[6], P. C. Weidenkaff[19], L. Wen[9], G. D. Westfall[34], H. Wieman[31], S. W. Wissink[25], R. Witt[59], Y. Wu[10], Z. G. Xiao[57], G. Xie[31], W. Xie[44], H. Xu[21], N. Xu[31], Q. H. Xu[49], Y. F. Xu[50], Y. Xu[49], Z. Xu[6], Z. Xu[9], C. Yang[49], Q. Yang[49], S. Yang[6], Y. Yang[37], Z. Yang[11], Z. Ye[45], Z. Ye[12], L. Yi[49], K. Yip[6], Y. Yu[49], H. Zbroszczyk[62], W. Zha[48], C. Zhang[52], D. Zhang[11], S. Zhang[48], S. Zhang[50], X. P. Zhang[57], Y. Zhang[48], Y. Zhang[11], Z. J. Zhang[37], Z. Zhang[6], Z. Zhang[12], J. Zhao[44], C. Zhong[50], C. Zhou[50], X. Zhu[57], Z. Zhu[49], M. Zurek[31], M. Zyzak[17]

[1]*Abilene Christian University, Abilene, Texas 79699*
[2]*AGH University of Science and Technology, FPACS, Cracow 30-059, Poland*
[3]*Alikhanov Institute for Theoretical and Experimental Physics NRC "Kurchatov Institute", Moscow 117218, Russia*
[4]*Argonne National Laboratory, Argonne, Illinois 60439*
[5]*American University of Cairo, New Cairo 11835, New Cairo, Egypt*
[6]*Brookhaven National Laboratory, Upton, New York 11973*
[7]*University of California, Berkeley, California 94720*
[8]*University of California, Davis, California 95616*
[9]*University of California, Los Angeles, California 90095*
[10]*University of California, Riverside, California 92521*
[11]*Central China Normal University, Wuhan, Hubei 430079*

[12]*University of Illinois at Chicago, Chicago, Illinois 60607*
[13]*Creighton University, Omaha, Nebraska 68178*
[14]*Czech Technical University in Prague, FNSPE, Prague 115 19, Czech Republic*
[15]*Technische Universität Darmstadt, Darmstadt 64289, Germany*
[16]*ELTE Eötvös Loránd University, Budapest, Hungary H-1117*
[17]*Frankfurt Institute for Advanced Studies FIAS, Frankfurt 60438, Germany*
[18]*Fudan University, Shanghai, 200433*
[19]*University of Heidelberg, Heidelberg 69120, Germany*
[20]*University of Houston, Houston, Texas 77204*
[21]*Huzhou University, Huzhou, Zhejiang 313000*
[22]*Indian Institute of Science Education and Research (IISER), Berhampur 760010 , India*
[23]*Indian Institute of Science Education and Research (IISER) Tirupati, Tirupati 517507, India*
[24]*Indian Institute Technology, Patna, Bihar 801106, India*
[25]*Indiana University, Bloomington, Indiana 47408*
[26]*Institute of Modern Physics, Chinese Academy of Sciences, Lanzhou, Gansu 730000*
[27]*University of Jammu, Jammu 180001, India*
[28]*Joint Institute for Nuclear Research, Dubna 141 980, Russia*
[29]*Kent State University, Kent, Ohio 44242*
[30]*University of Kentucky, Lexington, Kentucky 40506-0055*
[31]*Lawrence Berkeley National Laboratory, Berkeley, California 94720*
[32]*Lehigh University, Bethlehem, Pennsylvania 18015*
[33]*Max-Planck-Institut für Physik, Munich 80805, Germany*
[34]*Michigan State University, East Lansing, Michigan 48824*
[35]*National Research Nuclear University MEPhI, Moscow 115409, Russia*
[36]*National Institute of Science Education and Research, HBNI, Jatni 752050, India*
[37]*National Cheng Kung University, Tainan 70101*
[38]*Nuclear Physics Institute of the CAS, Rez 250 68, Czech Republic*
[39]*Ohio State University, Columbus, Ohio 43210*
[40]*Institute of Nuclear Physics PAN, Cracow 31-342, Poland*
[41]*Panjab University, Chandigarh 160014, India*
[42]*Pennsylvania State University, University Park, Pennsylvania 16802*
[43]*NRC "Kurchatov Institute", Institute of High Energy Physics, Protvino 142281, Russia*
[44]*Purdue University, West Lafayette, Indiana 47907*
[45]*Rice University, Houston, Texas 77251*
[46]*Rutgers University, Piscataway, New Jersey 08854*
[47]*Universidade de São Paulo, São Paulo, Brazil 05314-970*
[48]*University of Science and Technology of China, Hefei, Anhui 230026*
[49]*Shandong University, Qingdao, Shandong 266237*
[50]*Shanghai Institute of Applied Physics, Chinese Academy of Sciences, Shanghai 201800*
[51]*Southern Connecticut State University, New Haven, Connecticut 06515*
[52]*State University of New York, Stony Brook, New York 11794*
[53]*Instituto de Alta Investigación, Universidad de Tarapacá, Arica 1000000, Chile*
[54]*Temple University, Philadelphia, Pennsylvania 19122*
[55]*Texas A&M University, College Station, Texas 77843*
[56]*University of Texas, Austin, Texas 78712*
[57]*Tsinghua University, Beijing 100084*
[58]*University of Tsukuba, Tsukuba, Ibaraki 305-8571, Japan*
[59]*United States Naval Academy, Annapolis, Maryland 21402*
[60]*Valparaiso University, Valparaiso, Indiana 46383*
[61]*Variable Energy Cyclotron Centre, Kolkata 700064, India*
[62]*Warsaw University of Technology, Warsaw 00-661, Poland*
[63]*Wayne State University, Detroit, Michigan 48201 and*
[64]*Yale University, New Haven, Connecticut 06520*

(STAR Collaboration)

Non-monotonic variation with collision energy ($\sqrt{s_{NN}}$) of the moments of the net-baryon number distribution in heavy-ion collisions, related to the correlation length and the susceptibilities of the system, is suggested as a signature for the Quantum Chromodynamics (QCD) critical point. We report the first evidence of a non-monotonic variation in kurtosis times variance of the net-proton number (proxy for net-baryon number) distribution as a function of $\sqrt{s_{NN}}$ with 3.1σ significance, for head-on (central) gold-on-gold (Au+Au) collisions measured using the STAR detector at RHIC. Data in non-central Au+Au collisions and models of heavy-ion collisions without a critical point show a monotonic variation as a function of $\sqrt{s_{NN}}$.

One of the fundamental goals in physics is to understand the properties of matter when subjected to variations in temperature and pressure. Currently, the study of the phases of strongly interacting nuclear matter is the focus of many research activities worldwide, both theoretically and experimentally [1, 2]. The theory that governs the strong interactions is Quantum Chromodynamics (QCD), and the corresponding phase diagram is called the QCD phase diagram. From different examples of condensed-matter systems, experimental progress in mapping out phase diagrams is achieved by changing the material doping, adding more holes than electrons. Similarly it is suggested for the QCD phase diagram, that adding more quarks than antiquarks (the energy required is defined by the baryonic chemical potential, μ_B), through changing the heavy-ion collision energy, enables a search for new emergent properties and a possible critical point in the phase diagram. The phase diagram of QCD has at least two distinct phases: a Quark Gluon Plasma (QGP) at higher temperatures, and a state of confined quarks and gluons at lower temperatures called the hadronic phase [3–5]. It is inferred from lattice QCD calculations [6] that the transition is consistent with being a cross over at small μ_B, and that the transition temperature is about 155 MeV [7–9]. An important predicted feature of the QCD phase structure is a critical point [10, 11], followed at higher μ_B by a first order phase transition. Attempts are being made to locate the predicted critical point both experimentally and theoretically. Current theoretical calculations are highly uncertain about the location of the critical point. Lattice QCD calculations at finite μ_B face numerical challenges in computing [12, 13]. Within these limitations, the current best estimate from lattice QCD is that if there is a critical point, its location is likely above $\mu_B \sim 300$ MeV [12, 13]. The goal of this work is to search for possible signatures of the critical point by varying the collision energy in heavy ion collisions to cover a wide range in effective temperature (T) and μ_B in the QCD phase diagram [14].

Another key aspect of investigating the QCD phase diagram is to determine whether the system has attained thermal equilibrium. Several theoretical interpretations of experimental data have the underlying assumption that the system produced in the collisions should have come to local thermal equilibrium during its evolution. Experimental tests of thermalization for these femto-scale expanding systems are non-trivial. However, the yields of produced hadrons and fluctuations of multiplicity distributions related to conserved quantities have been studied and shown to have characteristics of thermodynamic equilibrium for higher collision energies [12, 15–20].

Upon approaching a critical point, the correlation length diverges and thus renders, to a large extent, microscopic details irrelevant. Hence observables like the moments of the conserved net-baryon number distribution, which are sensitive to the correlation length, are of interest when searching for a critical point. A non-monotonic variation of these moments as a function of $\sqrt{s_{NN}}$ has been proposed as an experimental signature of a critical point [10, 14]. However, considering the complexity of the system formed in heavy-ion collisions, signatures of a critical point are detectable only if they can survive the evolution of the system, including the effects of finite size and time [21]. Hence, it was proposed to study higher moments of distributions of conserved quantities (N) due to their stronger dependence on the correlation length [11]. The promising higher moments are the skewness, $S = \langle (\delta N)^3 \rangle / \sigma^3$, and kurtosis, $\kappa = [\langle (\delta N)^4 \rangle / \sigma^4] - 3$, where $\delta N = N - M$, M is the mean and σ is the standard deviation. The magnitude and the sign of the moments, which quantify the shape of the multiplicity distributions, are important for understanding the critical point [14, 22]. An additional crucial experimental challenge is to measure, on an event-by-event basis, all of the baryons produced within the acceptance of a detector [23–25]. However, theoretical calculations have shown that the proton-number fluctuations can also reflect the baryon-number fluctuations at the critical point [23, 26].

The measurements reported here are from Au+Au collisions recorded by the STAR detector [27] at RHIC from the years 2010 to 2017. The data is presented for $\sqrt{s_{NN}} =$ 7.7, 11.5, 14.5, 19.6, 27, 39, 54.4, 62.4 and 200 GeV as part of phase-I of the Beam Energy Scan (BES) program at RHIC [15]. These $\sqrt{s_{NN}}$ values correspond to μ_B values ranging from 420 MeV to 20 MeV at chemical freeze-out [15]. All valid Au+Au collisions occurring within 60 cm (80 cm for $\sqrt{s_{NN}}$ = 7.7 GeV) of the nominal interaction point along the beam axis are selected. For the results presented here, the number of minimum bias Au+Au collisions ranges between 3 million for $\sqrt{s_{NN}}$ = 7.7 GeV and 585 million at $\sqrt{s_{NN}} =$ 54.4 GeV. These statistics are found to be adequate to make the measurements of the moments of the net-proton distributions up to the fourth order [28]. The collisions are further divided into centrality classes characterised by their impact parameter, which is the closest distance between the centroid of two nuclei passing by. In practice, the impact parameter is determined indirectly from the measured multiplicity of charged particles other than protons (p) and anti-protons ($\bar{p}$) in the pseudo-rapidity range $|\eta| < 1$, where $\eta = -\ln[\tan(\theta/2)]$, with θ being the angle between the momentum of the particle and the positive direction of the beam axis. We exclude p and $\bar{p}$ while classifying events based on impact parameter specifically to avoid self-correlation effects [29]. The effect of self-correlation potentially arising due to the decay of heavier hadrons into $p(\bar{p})$ and other charged particles has been checked to be negligible from a study using standard heavy-ion collision event generators, HIJING [30] and UrQMD [31]. The effect of resonance decays and the pseudo-rapidity range for centrality determination have been understood and optimized using model calculations [32, 33]. The results presented here correspond to two event classes: central collisions (impact parameters $\sim$ 0-3 fm, obtained from the top 5% of the above-mentioned multiplicity distribution) and peripheral collisions (impact parameters $\sim$ 12-13 fm, obtained from the 70-80% region of the multiplicity distribution).

The protons and anti-protons are identified, along with their momenta, by reconstructing their tracks in the Time Projection Chamber (TPC) placed within a solenoidal magnetic field of 0.5 Tesla, and by measuring their ionization energy loss (dE/dx) in the sensitive gas-filled volume of the chamber. The selected kinematic region for protons covers all azimuthal angles for the rapidity range $|y| < 0.5$, where rapidity y is the
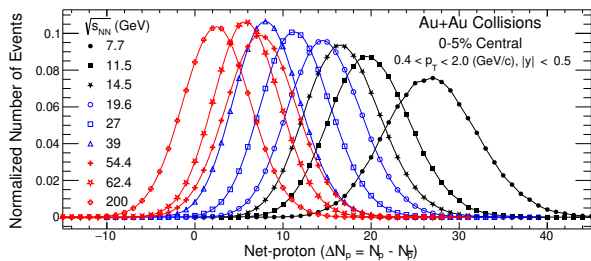
FIG. 1. Event-by-event net-proton number distributions for head-on (0-5% central) Au+Au collisions for nine $\sqrt{s_{NN}}$ values measured by STAR. The distributions are normalized to the total number of events at each $\sqrt{s_{NN}}$. The statistical uncertainties are smaller than the symbol sizes and the lines are shown to guide the eye. The distributions in this figure are not corrected for proton and anti-proton detection efficiency. The deviation of the distribution for $\sqrt{s_{NN}} = 54.4$ GeV from the general energy dependence trend is understood to be due to the reconstruction efficiency of protons and anti-protons being different compared to other energies.

inverse hyperbolic tangent of the component of speed parallel to the beam direction in units of the speed of light. The precise measurement of dE/dx with a resolution of 7% in Au+Au collisions allows for a clear identification of protons up to 800 MeV/c in transverse momentum (p_T). The identification for larger p_T (up to 2 GeV/c, with purity above 97%) is made by a Time Of Flight detector (TOF) [34] having a timing resolution of better than 100 ps. A minimum p_T threshold of 400 MeV/c and a maximum distance of closest approach to the collision vertex of 1 cm for each $p(\bar{p})$ candidate track is used to suppress contamination from secondaries and other backgrounds [15, 35]. This p_T acceptance accounts for approximately 80% of the total $p + \bar{p}$ multiplicity at mid-rapidity. This is a significant improvement from the results previously reported [35] which only had the $p + \bar{p}$ measured using the TPC. The observation of non-monotonic variation of the kurtosis times variance ($\kappa\sigma^2$) with energy is much more significant with the increased acceptance. For the rapidity dependence of the observable see Supplemental Material [34].

Figure 1 shows the event-by-event net-proton ($N_p - N_{\bar{p}} = \Delta N_p$) distributions obtained by measuring the number of protons (N_p) and anti-protons ($N_{\bar{p}}$) at mid-rapidity ($|y| < 0.5$) in the transverse momentum range $0.4 < p_T$ (GeV/c)< 2.0 for Au+Au collisions at various $\sqrt{s_{NN}}$. To study the shape of the event-by-event net-proton distribution in detail, cumulants (C_n) of various orders are calculated, where $C_1 = M$, $C_2 = \sigma^2$, $C_3 = S\sigma^3$ and $C_4 = \kappa\sigma^4$.

Figure 2 shows the net-proton cumulants (C_n) as a function of $\sqrt{s_{NN}}$ for central and peripheral (see Supplemental Material [34] for a zoomed version). Au+Au collisions. The cumulants are corrected for the multiplicity variations arising due to finite impact parameter range for the measurements [32]. These corrections suppress the volume fluctuations considerably [32, 36]. A different volume fluctuation correction method [37] has been applied to the 0-5% central Au+Au collision data and the results were found to be consistent with those shown in Fig 2 . The cumulants are also corrected for finite track reconstruction efficiencies of the TPC and TOF
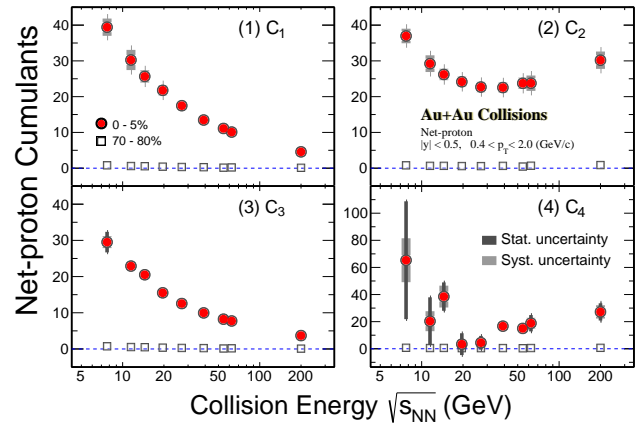

FIG. 2. Cumulants (C_n) of the net-proton distributions for central (0-5%) and peripheral (70-80%) Au+Au collisions as a function of collision energy. The transverse momentum (p_T) range for the measurements is from 0.4 to 2 GeV/c and the rapidity (y) range is -0.5 < y < 0.5.

detectors. This is done by assuming a binomial response of the two detectors [35, 38]. A cross-check using a different method based on unfolding [34] of the distributions for central Au+Au collisions at $\sqrt{s_{NN}} = 200$ GeV has been found to give values consistent with the cumulants shown in Fig. 2. Further, the efficiency correction method used has been verified in a Monte Carlo calculation. Typical values for the efficiencies in the TPC (TOF-matching) for the momentum range studied in 0-5% central Au+Au collisions at $\sqrt{s_{NN}} = 7.7$ GeV are 83%(72%) and 81%(70%) for the protons and anti-protons, respectively. The corresponding efficiencies for $\sqrt{s_{NN}} = 200$ GeV collisions are 62%(69%) and 60%(68%) for the protons and anti-protons, respectively. The statistical uncertainties are obtained using both a bootstrap approach [28, 38] and the Delta theorem [28, 38, 39] method. The systematic uncertainties are estimated by varying the experimental requirements to reconstruct p ($\bar{p}$) in the TPC and TOF. These requirements include the distance of the proton and anti-proton tracks from the primary vertex position, track quality reflected by the number of TPC space points used in the track reconstruction, the particle identification criteria passing certain selection criteria, and the uncertainties in estimating the reconstruction efficiencies. The systematic uncertainties at different collision energies are uncorrelated.

The large values of C_3 and C_4 for central Au+Au collisions show that the distributions have non-Gaussian shapes, a possible indication of enhanced fluctuations arising from a possible critical point [11, 22]. The corresponding values for peripheral collisions are small and close to zero. For central collisions, the C_1 and C_3 monotonically decrease with increasing $\sqrt{s_{NN}}$.

We employ ratios of cumulants in order to cancel volume variations to first order. Further, these ratios of cumulants are related to the ratio of baryon-number susceptibilities. The
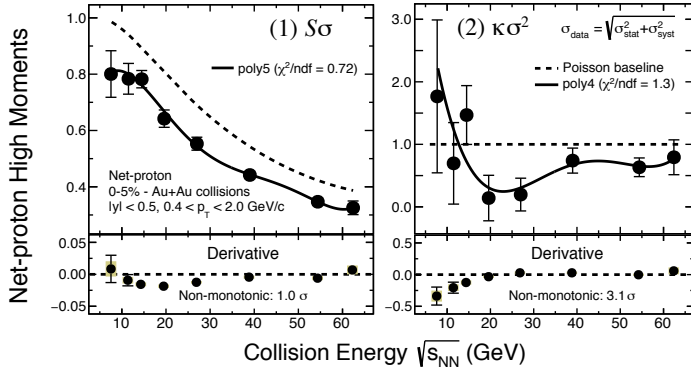
FIG. 3. Upper panels: $S\sigma$ (1) and $\kappa\sigma^2$ (2) of net-proton distributions for 0-5% central Au+Au collisions from $\sqrt{s_{NN}}$ = 7.7 - 62.4 GeV. The bar on the data points are statistical and systematic uncertainties added in quadrature. The black solid lines are polynomial fit functions which best describes the data. The black dashed lines are the Poisson baselines. Lower panels: Derivative of the fitted polynomial as a function of $\sqrt{s_{NN}}$. The bar and the shaded band on the derivatives represent the statistical and systematic uncertainties, respectively.

TABLE I. The p values of a χ^2 test between data and various models for the $\sqrt{s_{NN}}$ dependence of $S\sigma$ and $\kappa\sigma^2$ values of net-proton distributions in 0-5% central Au+Au collisions. The results are for the energy range 7.7 to 27 GeV which is relevant for the search for a critical point [12, 13].

Moments	HRG GCE	HRG EV (r = 0.5 fm)	HRG CE	UrQMD
$S\sigma$	< 0.001	< 0.001	0.0754	< 0.001
$\kappa\sigma^2$	0.00553	0.0450	0.0145	0.0221

latter are $\chi_n^B = \frac{d^n P}{d\mu_B^n}$, where n is the order and P is the pressure of the system at a given T and μ_B, computed in lattice QCD and QCD-based models [40]. The $C_3/C_2 = S\sigma$ $= (\chi_3^B/T)/(\chi_2^B/T^2)$ and $C_4/C_2 = \kappa\sigma^2 = (\chi_4^B)/(\chi_2^B/T^2)$. Close to the critical point, QCD-based calculations predict the net-baryon number distributions to be non-Gaussian and susceptibilities to diverge, causing moments, especially higher-order quantities like $\kappa\sigma^2$, to have non-monotonic variation as a function of $\sqrt{s_{NN}}$ [40, 41].

Figure 3 shows the central 0-5% Au+Au collision data for $S\sigma$ and $\kappa\sigma^2$ in the collision energy range of 7.7 – 62.4 GeV, fitted to a polynomial function of order five and four, respectively. The derivative of the polynomial function changes sign [34] with $\sqrt{s_{NN}}$ for $\kappa\sigma^2$, thereby indicating a non-monotonic variation of the measurement with the collision energy. The uncertainties of the derivatives are obtained by varying the data points randomly at each energy within the statistical and systematic uncertainties separately. The overall significance of the change in the sign of the slope for $\kappa\sigma^2$ versus $\sqrt{s_{NN}}$, based on the fourth order polynomial function fitting procedure from $\sqrt{s_{NN}}$ = 7.7 to 62.4 GeV, is 3.1σ. A similar exercise with the UrQMD [31] and HRG model with canonical ensemble [42] as the non-critical baseline yields an overall significance of 3.3σ. This significance is obtained by generating one million sets of points, where for each set, the measured $\kappa\sigma^2$ value at a given $\sqrt{s_{NN}}$ is randomly varied within the total Gaussian uncertainties (systematic and statistical uncertainties added in quadrature). Then for each new $\kappa\sigma^2$ versus $\sqrt{s_{NN}}$ set of points, a fourth order polynomial function is fitted and the derivative values are calculated at different $\sqrt{s_{NN}}$ (as discussed above). A total of 1143 sets were found to have the same derivative sign at all $\sqrt{s_{NN}}$. The probability that at least one derivative at a given $\sqrt{s_{NN}}$ has a different sign is found to be 0.998857, which corresponds to 3.1σ. A

similar procedure was applied to the lower-order product of moments. The σ^2/M (not shown) strongly favors a monotonic energy dependence excluding the non-monotonic trend at a 3.4 σ level. Within 1.0 σ significance the $S\sigma$ allows for a non-monotonic energy dependence. This is consistent with a QCD based model expectation that the higher the order of the moments the more sensitive it is to physics processes such as a critical point [11].

Figure 4 shows the variation of $S\sigma$ (or C_3/C_2) and $\kappa\sigma^2$ (or C_4/C_2) as a function of $\sqrt{s_{NN}}$ for central and peripheral Au+Au collisions. In central collisions, as discussed above, a non-monotonic variation with beam energy is observed for $\kappa\sigma^2$. The peripheral collisions on the other hand do not show a non-monotonic variation with $\sqrt{s_{NN}}$ around the statistical baseline of unity, and $\kappa\sigma^2$ values are always below unity. It is worth noting that in peripheral collisions, the system formed may not be hot and dense enough to undergo a phase transition or come close to the QCD critical point. The expectations from an ideal statistical model of hadrons assuming thermodynamic equilibrium, called the Hadron Resonance Gas (HRG) model [33], calculated within the experimental acceptance and considering a grand canonical ensemble (GCE), excluded volume (EV) [43], and canonical ensemble (CE) [42], are also shown in Fig. 4. The HRG results do not quantitatively describe the data. Corresponding $\kappa\sigma^2$ ($S\sigma$) results for 0-5% Au+Au collisions from a transport-based UrQMD model [31] calculation, which incorporates conservation laws and most of the relevant physics apart from a phase transition or a critical point, and which is calculated within the experimental acceptance, show a monotonic decrease (increase) with decreasing collision energy (see Supplemental Material [34] for a quantitative comparison). Similar conclusions are obtained from JAM [45], another microscopic transport model. Neither of the model calculations explains simultaneously the measured dependence of the $\kappa\sigma^2$ and $S\sigma$ of the net-proton distribution on $\sqrt{s_{NN}}$ for central Au+Au collisions. This can be seen from the values of a χ^2 test between the experimental data and various models for $\sqrt{s_{NN}}$ = 7.7 - 27 GeV given in Table I, p reflects the probability that a model agrees with the data.

In conclusion, we have presented measurements of net-proton cumulant ratios with the STAR detector at RHIC over a wide range of μ_B (20 to 420 MeV) which are relevant to a QCD critical point search in the QCD phase diagram. We have observed a non-monotonic behavior as a function of $\sqrt{s_{NN}}$, in net-proton $\kappa\sigma^2$ in central Au+Au collisions with a significance of 3.1σ relative to Skellam expectation. In contrast,
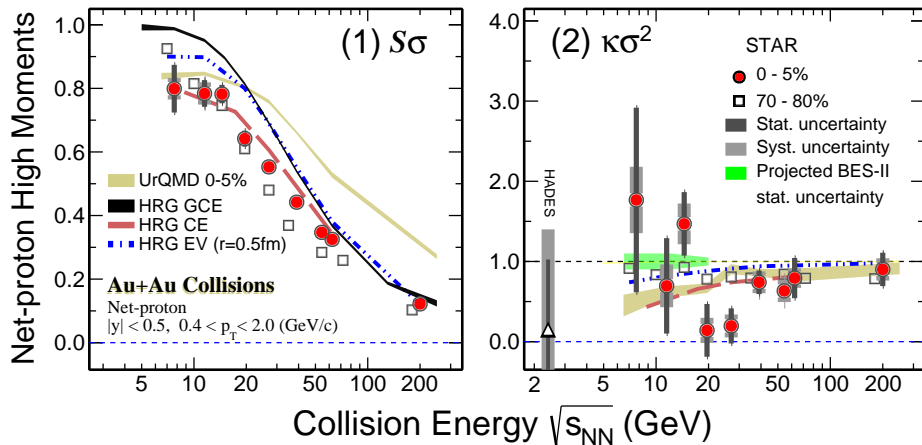
FIG. 4. $S\sigma$ (1) and $\kappa\sigma^2$ (2) as a function of collision energy for net-proton distributions measured in Au+Au collisions. The results are shown for central (0-5%, filled circles) and peripheral (70-80%, open squares) collisions within $0.4 < p_T$ (GeV/c) < 2.0 and $|y| < 0.5$. The vertical narrow and wide bars represent the statistical and systematic uncertainties, respectively. Shown as an open triangle is the result from the HADES experiment [44] for 0-10% Au+Au collisions and $|y| < 0.4$. The shaded green band is the estimated statistical uncertainty for BES-II. The peripheral data points have been shifted along the x-axis for clarity of presentation. Results from different variants (GCE, EV, CE) of the hadron resonance gas (HRG) model [33, 42, 43] and a transport model calculation (UrQMD [31]) for central collisions (0-5%) are shown as black, red, blue bands and a gold band, respectively.

monotonic behaviour with $\sqrt{s_{NN}}$ is predicted for the statistical hadron gas model, and for a nuclear transport model without a critical point, as observed experimentally in peripheral collisions. The deviation of the measured $\kappa\sigma^2$ from several baseline calculations with no critical point, and its non-monotonic dependence on $\sqrt{s_{NN}}$, are qualitatively consistent with expectations from a QCD-based model which includes a critical point [11, 14]. Our measurements can also be compared to the baryon-number susceptibilities computed from QCD to understand various other features of the QCD phase structure as well as to obtain the freeze-out conditions in heavy-ion collisions. Higher event statistics will allow for a more differential measurement of experimental observables in y-p_T. They will improve the comparison of the measurements with QCD calculations which include the dynamics associated with heavy-ion collisions, and hence they may help in establishing the critical point.

[1] A. Bzdak, S. Esumi, V. Koch, J. Liao, M. Stephanov and N. Xu, Phys. Rept. **853**, 1-87 (2020).

[2] X. Luo and N. Xu, Nucl. Sci. Tech. **28**, no.8, 112 (2017).

[3] K. Fukushima and T. Hatsuda, Rept. Prog. Phys. **74**, 014001 (2011).

[4] P. Braun-Munzinger and J. Wambach, Rev. Mod. Phys. **81**, 1031-1050 (2009).

[5] M. Asakawa and K. Yazaki, Nucl. Phys. A **504**, 668-684 (1989).

[6] Y. Aoki, G. Endrodi, Z. Fodor, S. D. Katz and K. K. Szabo, Nature **443**, 675-678 (2006).

[7] Y. Aoki, S. Borsanyi, S. Durr, Z. Fodor, S. D. Katz, S. Krieg and K. K. Szabo, JHEP **06**, 088 (2009).

[8] A. Bazavov, T. Bhattacharya, M. Cheng, C. DeTar, H. T. Ding, S. Gottlieb, R. Gupta, P. Hegde, U. M. Heller, F. Karsch, E. Laermann, L. Levkova, S. Mukherjee, P. Petreczky, C. Schmidt, R. A. Soltz, W. Soeldner, R. Sugar, D. Toussaint,

W. Unger and P. Vranas, Phys. Rev. D **85**, 054503 (2012).

[9] S. Gupta, X. Luo, B. Mohanty, H. G. Ritter and N. Xu, Science **332**, 1525-1528 (2011).

[10] M. A. Stephanov, K. Rajagopal and E. V. Shuryak, Phys. Rev. D **60**, 114028 (1999).

[11] M. A. Stephanov, Phys. Rev. Lett. **102**, 032301 (2009).

[12] A. Bazavov *et al.* [HotQCD], Phys. Rev. D **96**, no.7, 074510 (2017).

[13] A. Bazavov, H. T. Ding, P. Hegde, O. Kaczmarek, F. Karsch, E. Laermann, Y. Maezawa, S. Mukherjee, H. Ohno, P. Petreczky, H. Sandmeyer, P. Steinbrecher, C. Schmidt, S. Sharma, W. Soeldner and M. Wagner, Phys. Rev. D **95**, no.5, 054504 (2017).

[14] M. A. Stephanov, Phys. Rev. Lett. **107**, 052301 (2011).

[15] L. Adamczyk *et al.* (STAR Collaboration), Phys. Rev. C **96**, no.4, 044904 (2017).

[16] A. Andronic, P. Braun-Munzinger, K. Redlich and J. Stachel, Nature **561**, 321-330 (2018).

[17] G. A. Almasi, B. Friman and K. Redlich, Phys. Rev. D **96**, no.1, 014027 (2017).

[18] A. Bazavov, H. T. Ding, P. Hegde, O. Kaczmarek, F. Karsch, E. Laermann, S. Mukherjee, P. Petreczky, C. Schmidt, D. Smith, W. Soeldner and M. Wagner, Phys. Rev. Lett. **109**, 192302 (2012).

[19] S. Borsanyi, Z. Fodor, S. D. Katz, S. Krieg, C. Ratti and K. K. Szabo, Phys. Rev. Lett. **113**, 052301 (2014).

[20] S. Gupta, D. Mallick, D. K. Mishra, B. Mohanty and N. Xu, [arXiv:2004.04681 [hep-ph]].

[21] B. Berdnikov and K. Rajagopal, Phys. Rev. D **61**, 105017 (2000).

[22] M. Asakawa, S. Ejiri and M. Kitazawa, Phys. Rev. Lett. **103**, 262301 (2009).

[23] M. Kitazawa and M. Asakawa, Phys. Rev. C **86**, 024904 (2012).

[24] A. Bzdak and V. Koch, Phys. Rev. C **86**, 044904 (2012).

[25] A. Bzdak, V. Koch and V. Skokov, Phys. Rev. C **87**, no.1, 014901 (2013).

[26] Y. Hatta and M. A. Stephanov, Phys. Rev. Lett. **91**, 102003 (2003).

[27] K. H. Ackermann *et al.* (STAR Collaboration), Nucl. Instrum.

Meth. A **499**, 624-632 (2003).

[28] A. Pandav, D. Mallick and B. Mohanty, Nucl. Phys. A **991**, 121608 (2019).

[29] A. Chatterjee, Y. Zhang, J. Zeng, N. R. Sahoo and X. Luo, Phys. Rev. C **101**, no.3, 034902 (2020).

[30] X. N. Wang and M. Gyulassy, Phys. Rev. D **44**, 3501-3516 (1991).

[31] M. Bleicher, E. Zabrodin, C. Spieles, S. A. Bass, C. Ernst, S. Soff, L. Bravina, M. Belkacem, H. Weber, H. Stoecker and W. Greiner, J. Phys. G **25**, 1859-1896 (1999).

[32] X. Luo, J. Xu, B. Mohanty and N. Xu, J. Phys. G **40**, 105104 (2013).

[33] P. Garg, D. K. Mishra, P. K. Netrakanti, B. Mohanty, A. K. Mohanty, B. K. Singh and N. Xu, Phys. Lett. B **726**, 691-696 (2013).

[34] See Supplemental Material at [LINK] for event selection and proton identification, efficiency corrections using unfolding approach, zoomed version of peripheral collision data, rapidity dependence of cumulant ratio, quantitative comparison of data and model, and polynomial function fit to moment products.

[35] L. Adamczyk *et al.* (STAR Collaboration), Phys. Rev. Lett. **112**, 032302 (2014).

[36] T. Sugiura, T. Nonaka and S. Esumi, Phys. Rev. C **100**, no.4, 044904 (2019).

[37] P. Braun-Munzinger, A. Rustamov and J. Stachel, Nucl. Phys. A **960**, 114-130 (2017).

[38] X. Luo, Phys. Rev. C **91**, no.3, 034907 (2015).

[39] X. Luo, J. Phys. G **39**, 025008 (2012).

[40] R. V. Gavai and S. Gupta, Phys. Lett. B **696**, 459-463 (2011).

[41] B. Stokic, B. Friman and K. Redlich, Phys. Lett. B **673**, 192-196 (2009).

[42] P. Braun-Munzinger, B. Friman, K. Redlich, A. Rustamov and J. Stachel, [arXiv:2007.02463 [nucl-th]].

[43] A. Bhattacharyya, S. Das, S. K. Ghosh, R. Ray and S. Samanta, Phys. Rev. C **90**, no.3, 034909 (2014) and private communications 2020.

[44] J. Adamczewski-Musch *et al.* [HADES], Phys. Rev. C **102**, no.2, 024914 (2020).

[45] Y. Zhang, S. He, H. Liu, Z. Yang and X. Luo, Phys. Rev. C **101**, no.3, 034909 (2020).